Crystal and Electronic Structures of Magnesium(II), Copper(II), and Mixed Magnesium(II)−Copper(II) Complexes of the Quinoline Half of Styrylquinoline-Type HIV-1 Integrase Inhibitors

B. Courcot, D. Firley, B. Fraisse, P. Becker, and J.-M. Gillet

Ecole Centrale Paris, Laboratoire SPMS, UMR CNRS 8580 1, Grande Voie des Vignes, 92295 Châtenay-Malabry, France

P. Pattison and D. Chernyshov

Swiss-Norwegian Beam Lines at ESRF, 6 rue Jules Horowitz, BP 220, 38043 Grenoble, France

M. Sghaier

Equipe Matériaux et Santé, EA 401, Faculté de Pharmacie, Université Paris-Sud XI, 5 rue Jean-Baptiste Clément, 92296 Châtenay-Malabry, France

F. Zouhiri, D. Desmaële, and J. d'Angelo*

Laboratoire BIOCIS, UMR CNRS 8076, Faculté de Pharmacie, IFR 141, Université Paris-Sud XI, 5 rue Jean-Baptiste Clément, 92296 Châtenay-Malabry, France

F. Bonhomme, S. Geiger, and N. E. Ghermani*

Laboratoire PPB, UMR CNRS 8612, Faculté de Pharmacie, IFR 141, Université Paris-Sud XI, 5 rue Jean-Baptiste Clément, 92296 Châtenay-Malabry, France

Received: December 20, 2006; In Final Form: March 19, 2007

A new target in AIDS therapy development is HIV-1 integrase (IN). It was proven that HIV-1 IN required divalent metal cations to achieve phosphodiester bond cleavage of DNA. Accordingly, all newly investigated potent IN inhibitors contain chemical fragments possessing a high ability to chelate metal cations. One of the promising leads in the polyhydroxylated styrylquinolines (SQLs) series is (*E*)-8-hydroxy-2-[2-(4,5-dihydroxy-3-methoxyphenyl)-ethenyl]-7-quinoline carboxylic acid (**1**). The present study focuses on the quinoline-based progenitor (**2**), which is actually the most probable chelating part of SQLs. Conventional and synchrotron low-temperature X-ray crystallographic studies were used to investigate the chelating power of progenitor **2**. Mg^{2+} and Cu^{2+} cations were selected for this purpose, and three types of metal complexes of **2** were obtained: Mg(II) complex (**4**), Cu(II) complex (**5**) and mixed Mg(II)−Cu(II) complexes (**6** and **7**). The analysis of the crystal structure of complex **4** indicates that two tridentate ligands coordinate two Mg^{2+} cations, both in octahedral geometry. The Mg−Mg distance was found equal to 3.221(1) Å, in agreement with the metal−metal distance of 3.9 Å encountered in the crystal structure of *Escherichia coli* DNA polymerase I. In **5**, the complex is formed by two bidentate ligands coordinating one copper ion in tetrahedral geometry. Both mixed Mg(II)−Cu(II) complexes, **6** and **7** exhibit an original arrangement of four ligands linked to a central heterometallic cluster consisting of three octahedrally coordinated magnesium ions and one tetrahedrally coordinated copper ion. Quantum mechanics calculations were also carried out in order to display the electrostatic potential generated by the dianionic ligand **2** and complex **4** and to quantify the binding energy (BE) during the formation of the magnesium complex of progenitor **2**. A comparison of the binding energies of two hypothetical monometallic Mg(II) complexes with that found in the bimetallic magnesium complex **4** was made.

Introduction

Acquired immunodeficiency syndrome (AIDS) is one of the greatest challenges to humankind. All oral agents licensed to treat HIV-1 diseases target two of the three essential, virally encoded enzymes, reverse transcriptase (RT), and protease (PR).[1] However, although the advent of combination therapy with HIV-1 RT and PR inhibitors has made it possible to suppress the replication of the virus in infected persons to such an extent that it becomes almost undetectable in the plasma for more than 2 years, HIV-1 persists in sanctuaries such as peripheral blood mononuclear cells or resting T-lymphocytes. This means that AIDS can be temporarily controlled, but not eradicated with current treatments.[2−4] Therefore, additional therapeutic approaches are warranted. One such approach is to

* Corresponding author. E-mail: noureddine.ghermani@u-psud.fr. Telephone: +33 (0)1 46 83 56 48. Fax: +33 (0)1 46 83 58 82.

10.1021/jp0687551 CCC: $37.00
Published on Web 05/09/2007

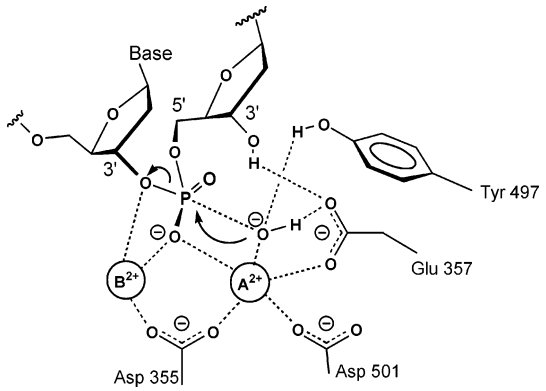

Figure 1. The proposed transition state of the "two-metal-ion" enzymatic mechanism for the 3′-5′ exonuclease reaction. The putative role of metal A is to facilitate the formation of an attacking hydroxide ion. Metal B is hypothesized to facilitate the leaving of the 3′-hydroxide group.

target the third viral enzyme, integrase (IN), that inserts the viral DNA into the host cellular genome through a multistep process that includes two catalytic reactions. These comprise the 3′-endonucleolytic processing of both ends of the transcribed viral DNA consisting of the excision of a dinucleotide adjacent to a conserved CA sequence and the joining of the 3′-processed viral and host chromosomal DNAs (strand transfer).[5−10] Both reactions are essential for the life cycle of the virus. However, since the half-life for the hydrolysis of DNA phosphodiester bond at neutrality far exceeds the life span of a human,[11] highly efficient catalytic process is required to provide the critical 10^{16}-fold rate enhancement needed to cleave this bond on the biological time scale.[12] In this respect, the "two-metal-ion" enzymatic mechanism, first formulated by Beese and Steitz for the 3′−5′ exonuclease reaction of the Klenow fragment of *Escherichia coli* DNA polymerase I, appears fully capable of providing the necessary rate enhancement.[13] A refined X-ray crystal structure of this protein reveals a distorted tetrahedral geometry for metal site A and an octahedral coordination for the second metal B that is 3.9 Å from the first. It has been suggested that the difficult phosphodiester bond cleavage is promoted by the two divalent cations that operate in concert. The metal ion in site A initiates the formation of the hydroxide ion, which may be functioning as a Lewis acid by displacing a proton from water. Metal ion B directly ligates the leaving group atom, thereby facilitating the bond breakage step by neutralizing the developing negative charge on this oxygen anion. The identity of the metal ions that are bound in vivo was not specified. However, crystal soaking experiments in the presence of both Zn^{2+} and Mg^{2+} ions show that Zn^{2+} binds to site A and Mg^{2+} to site B, an observation consistent with the preferred coordination geometry of these metal ions, tetrahedral for zinc and octahedral for magnesium ions, that is exhibited by sites A and B, respectively (Figure 1). This mechanism has become very popular since it may be applicable to a large variety of polynucleotidyl transferases, including HIV-1 IN.[14−18] The crystal structure of Mg(II)-complexed core domain of HIV-1 IN shows that one Mg^{2+} ion is coordinated by two of the three critical active site residues (Asp-64 and Asp-116).[19] However, recent studies of molecular dynamics,[20] drug docking in the active site of the enzyme,[17] and binding of metal cations to the catalytic core domain of the avian sarcoma virus IN[15] suggest that HIV-1 IN could require linking of an additional divalent metal cation by the third amino acid of the catalytic triad (Glu-152) to achieve integration. It is probable that the second ion binds only in the presence of the DNA substrate.[10,16,19]

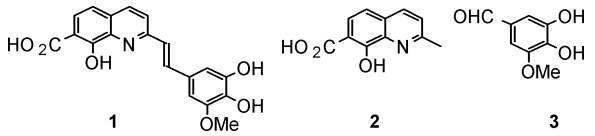

Figure 2. Structures of styrylquinoline **1** and its progenitors **2** and **3**.

On the basis of these observations, one of our laboratories has developed a new class of polyhydroxylated styrylquinolines (SQLs), which were designed to chelate divalent metal ion(s) operating in the catalytic core domain of HIV-1 IN. SQLs, exemplified by **1**, which results from the Perkin-type condensation between the progenitors **2** (HMQCA, stands for 8-hydroxy-2-methyl-quinoline-7-carboxylic acid) and **3** (Figure 2), are potent HIV-1 IN inhibitors in in vitro experiments, block the replication of HIV-1 in cell culture and are devoid of cytotoxicity.[21−34] These properties make SQLs promising candidates for the development of therapeutic HIV-1 IN inhibitors. One possible mechanism of action of SQLs is that they block the polynucleotide binding and catalytic site of HIV-1 IN through functional sequestration of the critical Mg^{2+} cofactor by their salicylic acid part.[22] With the aim to support this hypothesis, the complexing ability of SQLs for divalent metal ions was verified through further experiments including the elaboration and crystallographic characterization of SQLs−divalent metal complexes. However, attempts to solve the crystal structure of a variety of divalent metal complexes of **1** having proved invariably unsuccessful, we have explored the corresponding complexes of progenitor **2**, bearing in mind that previous structure−activity relationship studies[22] and docking procedures[23,24,31] have identified the salicylic acid moiety of the quinoline half of SQLs as a critical pharmacophore for antiviral activity. The complexation of **2** by Mg^{2+} ion, the presumed relevant cofactor for integration of the transcribed HIV-1 DNA in mammalian cells, was investigated first (complex **4**). Crystallographic characterization of tetrahedrally coordinated copper complex of **2** (**5**) was next investigated, keeping in mind that such a geometry is postulated for metal site A in the aforementioned "two-metal-ion" enzymatic mechanism (Figure 1). Since the metal sites A and B exhibit tetrahedral and octahedral geometries, respectively, preparation and characterization of a mixed Mg(II)−Cu(II) complex of **2** (**6**) were also investigated. Another crystallization procedure using DMSO as a solvent yields a similar structure of a mixed Mg(II)−Cu(II) complex of **2** (**7**). Finally, in order to quantify the metal-chelating property of progenitor **2**, the Mg-binding energies of complex **4** and hypothetical monomagnesium complexes were carried out through quantum mechanic calculations at the DFT level of theory.

Experimental and Computational Section

Synthesis of the Complexes: Materials and Measurements. HMQCA (**2**) was prepared according to the literature.[21] Elemental analyses (C, H and N) were performed on a Perkin-Elmer 2400 analyzer. Thermal analyses (TG-DTA) were carried out using a TGA7 Perkin-Elmer thermal analyzer under N_2. The IR spectra were recorded with Bruker Vector 22 spectrometer.

Synthesis of $[Mg_2(HMQCA)_2(H_2O)_4](H_2O)_2$ (4). HMQCA (305 mg, 1.5 mmol) and $Mg(OH)_2$ (106 mg, 1.8 mmol) were heated under reflux in a mixture of acetone (12 mL) and water (6 mL) for 3 h. The solvents were removed under vacuo, and the residue was dissolved in DMF (10 mL). The excess of $Mg(OH)_2$ was filtered off, DMF was removed under vacuo, and small cream-colored crystals were obtained by addition of water (ca 10 mL). The crystals were filtered off and dried at room

TABLE 1: Crystallographic Data and Refinement Details for Complexes 4−7

	4	5	6	7
chemical formula	$Mg_2[C_{11}H_7NO_3]_2 \cdot 6H_2O$	$Cu[C_{11}H_8NO_3]_2 \cdot 2H_2O$	$Mg_3Cu[C_{11}H_7NO_3]_4 \cdot 8H_2O$	$Mg_3Cu[C_{11}H_7NO_3]_4 \cdot 10\ H_2O \cdot 3(CH_3)_2SO$
molar weight (g.mol^{-1})	559.07	503.94	1085.3	1355.2
cell setting, space group	orthorhombic *Pbca*	monoclinic $P2_1/c$	triclinic *P*-1	triclinic *P*-1
a (Å)	13.3445(5)	7.3478(3)	12.333(1)	12.590(6)
b (Å)	7.5904(3)	17.1948(7)	12.496(1)	13.309(6)
c (Å)	24.1082(9)	17.4944(7)	15.156(2)	18.796(9)
α (deg)	90.0	90.0	93.807(9)	70.34(1)
β (deg)	90.0	114.835(1)	93.545(8)	84.27(1)
γ (deg)	90.0	90.0	109.351(9)	81.08(1)
V (Å^3)	2441.9	2005.9	2190.2	2926.1
Z	4	4	2	2
ρ_{calc} (Mg m^{-3})	1.52	1.67	1.65	1.55
λ (Å)	0.80000	0.71069	0.71000	0.71069
μ (mm^{-1})	0.17	1.15	0.63	0.60
T (K)	120(1)	100(1)	120(1)	100(1)
(sin θ/λ)max (Å^{-1})	0.82	0.69	0.75	0.70
measured reflections	5326	13617	12916	20632
unique reflections	4838	5019	7445	14417
R_{int}; $R\sigma$ (%)	4.50; 13.20	2.34; 2.89	3.50; 4.29	2.39; 5.68
$R1(F_o > 4(F_o))$ (%)	3.77	2.98	4.50	8.82
*wR*2 (%); S	9.87; 0.844	7.26; 1.052	10.23; 1.072	25.18; 1.032
reflections used ($F_o > 4\sigma(F_o)$)	1979	4535	6290	10669
no of parameters	214	320	700	751
$(\Delta/\sigma)_{max}$	0.001	-0.001	0.001	0.001
$\Delta\rho_{max}$, $\Delta\rho_{min}$ (iÅ^{-3})	0.49, -0.34	0.34, -0.63	0.41, -0.38	4.23, -2.50

temperature under vacuo (20 Torr) over anhydrous calcium sulfate. Yield: 302 mg (70%). Elemental analysis calcd (%) for $C_{22}H_{26}N_2Mg_2O_{12}$: C 47.26, H 4.65, N 5.01. Found: C 46.75, H 4.87, N 4.99. Thermal study (TG-DTA) reveals a weight loss of 19.7% at 30−180 °C corresponding to the loss of six water molecules (calc. 19.3%). IR (neat, cm^{-1}): 3344 (m), 1647 (m), 1604 (m), 1560 (s), 1524 (s), 1459 (s), 1434 (s), 1367 (s), 1330 (s), 1293 (m), 1267 (s), 1203 (m), 1163 (m), 1113 (s), 915 (m), 841 (s), 764 (s), 744 (s), 687 (m), 658 (m), 608 (m).

Synthesis of [Cu(HMQCA)(H$_2$O)](H$_2$O) (5). HMQCA (102 mg, 0.5 mmol) was dissolved in 1N NaOH (0.5 mL, 0.5 mmol). A solution of $CuCl_2 \cdot 2H_2O$ (43 mg, 0.25 mmol) in water (ca 2 mL) was added, resulting in the immediate formation of dark brown crystals. The crystals were filtered off, successively washed with acetic acid and water, and dried at room temperature under vacuo (20 Torr) over anhydrous magnesium sulfate. Yield: 115 mg (91%). Elemental analysis calcd (%) for $C_{22}H_{20}N_2CuO_8$: C 52.43, H 4.00, N 5.56. Found: C 52.31, H 3.86, N 5.50. IR (neat, cm^{-1}): 2765 (m), 1736 (s), 1709 (s), 1558 (m), 1512 (m), 1454 (s), 1409 (s), 1340 (m), 1273 (m), 1230 (s), 1157 (m), 1127 (m), 1110 (m), 1027 (m), 961 (m), 872 (m), 860 (m), 826 (m), 812 (m), 750 (s), 710 (m), 667 (m), 589 (s), 571 (m).

Synthesis of [Mg$_3$Cu(HMQCA)$_4$(H$_2$O)$_4$](H$_2$O)$_4$ (6). Complex **4** (59 mg, 0.105 mmol) and $CuCl_2 \cdot 2H_2O$ (9.2 mg, 0.054 mmol) were dissolved in DMF (ca 1 mL) and the mixture was concentrated under reduced pressure. THF (ca 1 mL) and water (ca 1 mL) were added to the residue, giving a beige microcrystalline powder. Small dark red crystals of **6** were selected for X-ray study. However, because of the heterogeneity of the powder, no additional analytical investigations were undertaken.

Synthesis of [Mg$_3$Cu(HMQCA)$_4$(H$_2$O)$_3$(DMSO)](H$_2$O)$_7$-(DMSO)$_2$ (7). Complex **4** (203 mg, 0.36 mmol) and $CuCl_2 \cdot 2H_2O$ (34 mg, 0.20 mmol) were dissolved in DMSO (5 mL). Water (5 mL) was added and the solution was kept in a refrigerator overnight. Dark red prismatic crystals of **7** were obtained. Complexes **6** and **7** mostly differ in the nature and the number of associated solvent molecules (8 water molecules in **6**, 3 DMSO molecules and 10 water molecules in **7**). Crystals of complex **7** were dried at room temperature under vacuo (20 Torr) over anhydrous magnesium sulfate, furnishing an ocher powder. Yield: 150 mg (70%). Elemental analysis calcd (%) for $C_{50}H_{48}N_4S_3Mg_3CuO_{16}$ [corresponding to $Mg_3Cu(HMQCA)_4(H_2O)(DMSO)_3$, since nine water molecules are lost during drying]: C 50.29, H 4.05, N 4.69; found: C 50.13, H 4.14, N 4.51; thermal study (TG-DTA) reveals a total weight loss of 20.7% at 50−460 °C (7.5% at 50−190 °C and 13.2% at 290−460 °C) corresponding to the loss of one water molecule and three DMSO molecules (calc. 21.1%). IR (neat, cm^{-1}): 3080 (m), 1586 (s), 1506 (s), 1432 (s), 1364 (s), 1321 (m), 1295 (m), 1248 (s), 1220 (m), 1162 (m), 1144 (m), 1106 (s), 1042 (m), 912 (m), 831 (s), 752 (s), 730 (s), 658 (m), 610 (m).

Crystallographic Studies. Single crystal analyses were performed on selected samples of complexes **4**−**7** (Table 1). Despite sustained efforts directed toward the crystallization of **4** and **6**, the prismatic plate-like crystals obtained had dimensions not exceeding 100 μm in width and 50 μm in thickness. An intense X-ray source was therefore required to perform diffraction experiments. The single-crystal data for complexes **4** and **6** were thus collected at the Swiss-Norwegian Beamline at the ESRF. A highly monochromatic synchrotron radiation with wavelengths $\lambda = 0.8000$ Å for **4** and 0.7100 Å for **6** was chosen for the data collections, carried out at 120 K. For complexes **5** and **7**, the dimensions of the crystals allowed us to collect the data at 100 K on an in-house Siemens Smart CCD diffractometer with Mo Kα radiation. The crystal of **7** used in the present study was mounted and sealed in a glass capillary because of its instability in air.

The structures of complexes **4**−**7** were solved by direct methods (program SIR97[35]) and refined by full-matrix least-squares on F^2 (program SHELXL-97[36]). All non-hydrogen atoms were refined anisotropically. The hydrogen atoms were located from difference Fourier maps and, when applicable, were refined using the riding atom model. The position of the water hydrogen and hydroxyl hydrogen atoms were refined using bond distances constraints O−H = 0.85(1) Å and for water molecules, H−H = 1.37(2) Å. All calculations were performed using the WinGx suite of programs.[37] The well-faceted pyramidal crystals obtained for complex **5** were, however, systematically twinned. Although the diffraction data for **5** was initially indexed in an orthorhombic unit-cell, no structure solution was forthcoming in this crystal system. The structure was then solved using the

TABLE 2: Selected Bond Lengths, Interatomic Distances [Å], and Angles [deg] for 4−7[a]

complex **4**			
Mg−O3	2.055(2)	Ow1−Mg−Ow2	162.56(8)
Mg−N	2.326(2)	Ow1−Mg−O3	89.45(6)
Mg−Ow1	2.068(2)	Ow1−Mg−N	84.77(7)
Mg−Ow2	2.044(2)	O3−Mg−N	73.74(6)
Mg−O2#1	2.073(2)	N−Mg−O2#1	126.64(7)
Mg−O3#1	2.023(1)	O2#1−Mg−O3#1	84.12(6)
Mg−Mg#1	3.220(1)		
complex **5**			
Cu−O3	1.995(1)	Ow1−Cu−O3	133.71(6)
Cu−O31	2.045(1)	Ow1−Cu−N	91.49(9)
Cu−N	1.995(2)	O3−Cu−O31	124.72(6)
Cu−N1	2.001(2)	O3−Cu−N	82.94(7)
Cu−Ow1	2.107(2)	O31−Cu−N1	82.39(7)
		N−Cu−N1	176.78(7)
complex **6**			
Cu−O3	1.970(2)	O3−Cu−O31	142.0(1)
Cu−O31	1.966(2)	O3−Cu−N	83.29(9)
Cu−N	2.015(2)	O3−Cu−N1	115.49(8)
Cu−N1	2.013(3)	O31−Cu−N	119.70(8)
		O31−Cu−N1	83.8(1)
		N−Cu−N1	114.6 (1)
Mg1−Ow1	2.019(3)	Ow1−Mg1−O3	169.40(9)
Mg1−O2	1.983(2)	Ow1−Mg1−O2	84.4 (1)
Mg1−O3	2.030(3)	O2−Mg1−O23	95.80(9)
Mg1−O23	2.229(2)	O32−Mg1−N2	75.08(8)
Mg1−O32	1.996(2)	O23−Mg1−O32	76.31(7)
Mg1−N2	2.293(2)	O2−Mg1−N2	113.01(9)
Mg2−Ow21	2.073(3)	Ow21−Mg2−O33	172.15(9)
Mg2−Ow22	2.072(3)	Ow21−Mg2−Ow22	83.2(1)
Mg2−O22	2.056(2)	Ow22−Mg2−O23	94.71(8)
Mg2−O23	2.097(2)	O23−Mg2−O32	79.66(8)
Mg2−O32	1.986(2)	O22−Mg2−O32	84.97(8)
Mg2−O33	1.995(2)	O22−Mg2−Ow22	102.75(8)
Mg3−Ow3	2.087(2)	Ow3−Mg3−O22	99.6 (1)
Mg3−O21	1.958(2)	O21−Mg3−O31	86.01(8)
Mg3−O22	2.157(2)	Ow3−Mg3−O21	88.61(8)
Mg3−O31	2.072(3)	O31−Mg3−O33	90.64(8)
Mg3−O33	1.993(2)	Ow3−Mg3−O33	95.68(9)
Mg3−N3	2.305(3)	O22−Mg3−N3	151.71(8)
Cu−Mg1	3.454(1)	Mg1−Mg2	3.213(1)
Cu−Mg3	3.506(1)	Mg2−Mg3	3.184(1)
complex **7**			
Cu−O3	1.916(3)	O3−Cu−O31	164.1(1)
Cu−O31	1.911(3)	O3−Cu−N	82.6(2)
Cu−N	2.094(4)	O3−Cu−N1	106.6(2)
Cu−N1	2.095(3)	O31−Cu−N	105.6(2)
		O31−Cu−N1	82.5(1)
		N−Cu−N1	114.9(2)
Cu−Mg1	3.320(2)	Mg1−Mg2	3.189(3)
Cu−Mg3	3.305(2)	Mg2−Mg3	3.170(2)

[a] Symmetry code for complex **4**: #1 $-x+1, -y, -z+2$.

orthorhombic metric and a triclinic symmetry, space group *P*-1. The true symmetry of this structure was then found to be monoclinic, space group $P2_1/c$ (program ADDSYM in PLATON[38]). After the appropriate transformations, the structure was refined in $P2_1/c$ down to R1 = 21%, at which stage a twinning law revealed by ROTAX[39] (180° rotation about the [1 0 0] direction) was included in the model. The refinement then proceeded smoothly down to R1 = 2.98%.

Computational Methods. Ab initio single molecule calculations in gas phase were performed using the program Gaussian 03[40] with DFT[41,42] B3LYP/6-31G+(d,p) basis set.[43,44] These calculations were carried out on potent inhibitor **1** and ligand **2** in their dianionic state, on complex **4** and derived hypothetical monomagnesium complexes of **2**. The binding energies (BE) were also estimated for the dimagnesium complex **4**.

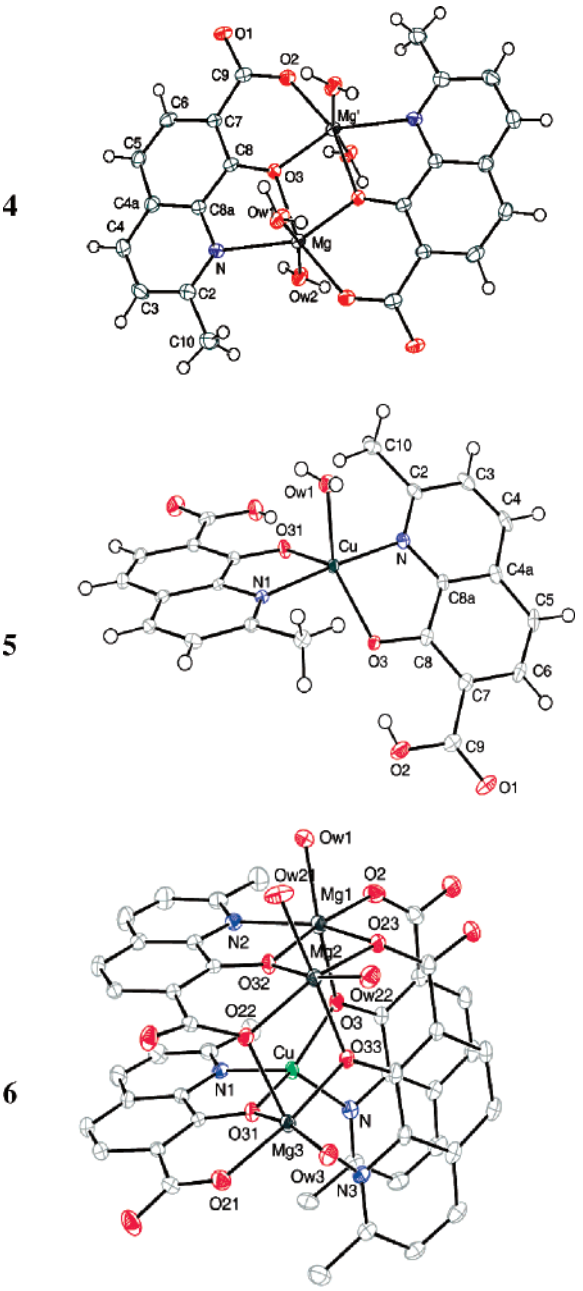

Figure 3. X-ray structures of metal complexes **4**, **5**, and **6** of progenitor **2**. Symmetry code for the second ligand in **4**: $-x+1, -y, -z+2$.

Results and Discussion

Crystal Structures. In Table 2 are given the main bond lengths and angles for the complexes **4**−**7** of progenitor **2** (see Figure 3 for the atom labeling). The dimagnesium complex **4** crystallizes in *Pbca* orthorhombic space group. The molecular structure of complex **4** is depicted in Figure 3. Two tridentate ligands coordinate two Mg^{2+} cations via the carboxylato O2-atom, the phenoxo O3-atom and the quinoline nitrogen atom. N and O2 atoms are linked to one Mg^{2+} ion whereas O3 is bonded to the two metal atoms. Such an architecture gives rise to a center of inversion located between the two metal cations and a head-to-tail planar arrangement of the ligands. Two water molecules fulfill the octahedral coordination of each Mg^{2+} ion in the apical positions. Two other water molecules per complex

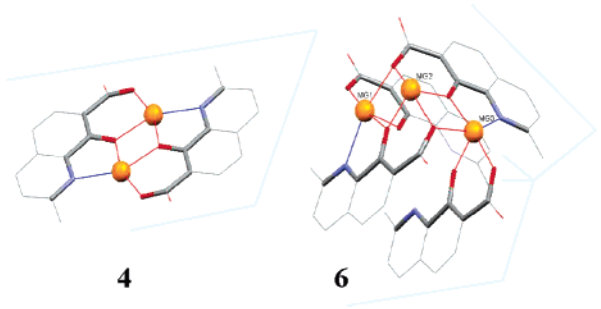

Figure 4. Sequestration of magnesium cations by progenitor **2** in complexes **4** and **6**. Magnesium cations are represented as spheres; hydrogen, copper, and water oxygen atoms are omitted for clarity.

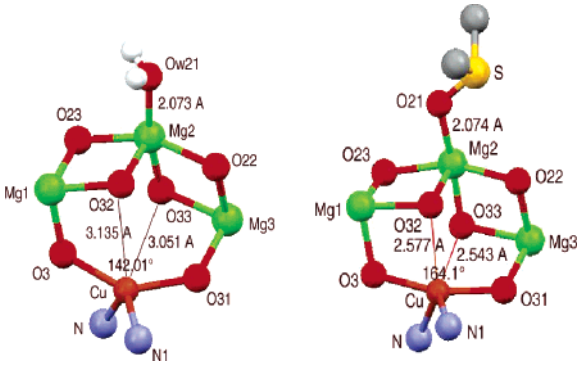

Figure 5. The O-bridged heterometallic cores of complexes **6** (left) and **7** (right).

(not shown in Figure 3) are present in the crystal lattice and link the complex units via multiple hydrogen bonds involving both O1 and O2 atoms. The structure of complex **4** is original compared to those of related molecules. For instance, tridentate chelating molecules such as 8-hydroxyquinaldinic acid and 8-hydroxyquinoline-2-carboxylic acid form monometallic complexes with divalent metal ions like Ni^{2+} and Co^{2+}.[45,46] In both cases, the two ligands are perpendicular to each other in order to satisfy the octahedral coordination of the metal. However, bimetallic cores have been observed in the crystal structures of several metal complexes related to **4**, e.g., Mg(II)-complexed ferron,[47] Mn(III) complex of salicylic acid,[48] and Cu(II) complex of 4-(1′-carboxy-2′-oxopropylidene)-2,2,5,5-tetramethyl-3-imidazolidine-1-oxyl.[49]

Complex **5** crystallizes in the monoclinic space group $P2_1/c$. The ORTEP[50] plot of this complex is shown in Figure 3. The complex is formed by two head-to-tail bidentate organic ligands coordinating the Cu^{2+} ion. In this case, the phenoxo O3-atoms (O3 and O31) and the quinoline nitrogen atoms (N and N1) of the two ligands are preferentially linked to the copper atom, forming a distorted tetrahedron. The particularity of this coordination is that the N−Cu−N1 bond is quasi linear displaying an angle of 176.78(7)°. The angle between the two connected ligand planes is 131.3(2)°. One water molecule is linked to the copper atom with a Cu−Ow1 distance of 2.107(2) Å giving rise to a penta-coordination of the metal. Another lattice water molecule was found in the asymmetric unit. A similar structure was found for the aquabis(quinoline-2-carboxylato-κ^2N,O)zinc(II) complex by Okabe and Muranishi.[51] Contrary to complex **4**, the carboxylato O2-atoms of both ligands are protonated and their H atoms are involved in intramolecular hydrogen bonds with the phenoxo O3-atoms. This unusual coordination mode clearly reflects the marked propensity of a basic nitrogen atom to bind Cu^{2+} (a "soft" cation).[52] It is noteworthy that (salicylato)metal complexes in which the $salH^-$ ligand arises by deprotonation of the hydroxyl rather than the carboxyl proton and so involves the $HO_2CC_6H_4O^-$ anion are scarce, the first reported example is $[MoO_2(salH)(sal)](pyH)$.[53]

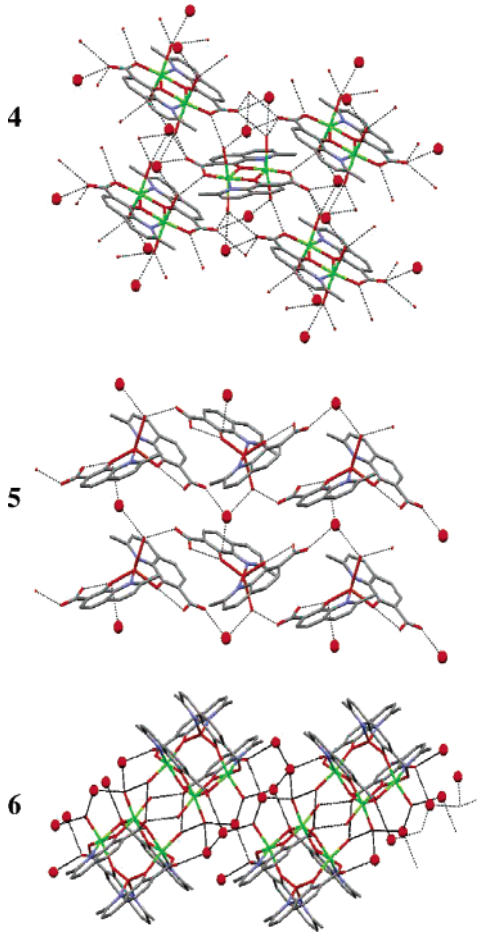

Figure 6. Hydrogen bond networks in the crystal lattices of **4**, **5**, and **6**. Only extra water molecule oxygen atoms are represented as spheres; hydrogen atoms are omitted for clarity.

Complex **6** crystallizes in the triclinic system, space group *P*-1. A supramolecular unit built-up by four organic ligands coordinating three Mg^{2+} and one Cu^{2+} cations is observed. Cu^{2+} is tetrahedrally coordinated whereas the three Mg^{2+} cations are in octahedral geometry. The remaining carboxylato O2-atoms (O2 and O21) of two ligands coordinate two magnesium cations (Mg1 and Mg3), each of them involving one water molecule (Ow1 and Ow3) and the two other organic ligands to fulfill their octahedral coordination. A third magnesium ion (Mg2), harnessed to two water molecules (Ow21 and Ow22 in Figure 3), connects these two latter ligands leading to a cage structure. In this supramolecular unit, the ligands are grouped by pairs facing one another in parallel planes. Consequently, Mg2 is exclusively connected to six oxygen atoms whereas Mg1 and Mg3 are both linked to five oxygen atoms and one nitrogen atom. Four extra water molecules are present in the asymmetric unit. All water molecules, connected or not to Mg^{2+} cations, participate to an infinite network of hydrogen bonds linking together the complex units in the crystal.

Complex **7** crystallizes in *P*-1 triclinic space group. As in complex **6**, the same supramolecular assembly was obtained with 3 Mg^{2+} and one Cu^{2+} cations connected through four ligands **2**. Molecular structure of **7** (not depicted in Figure 3) is very similar to that of **6**, with exception of the nature and the number of associated solvent molecules. Ten water molecules

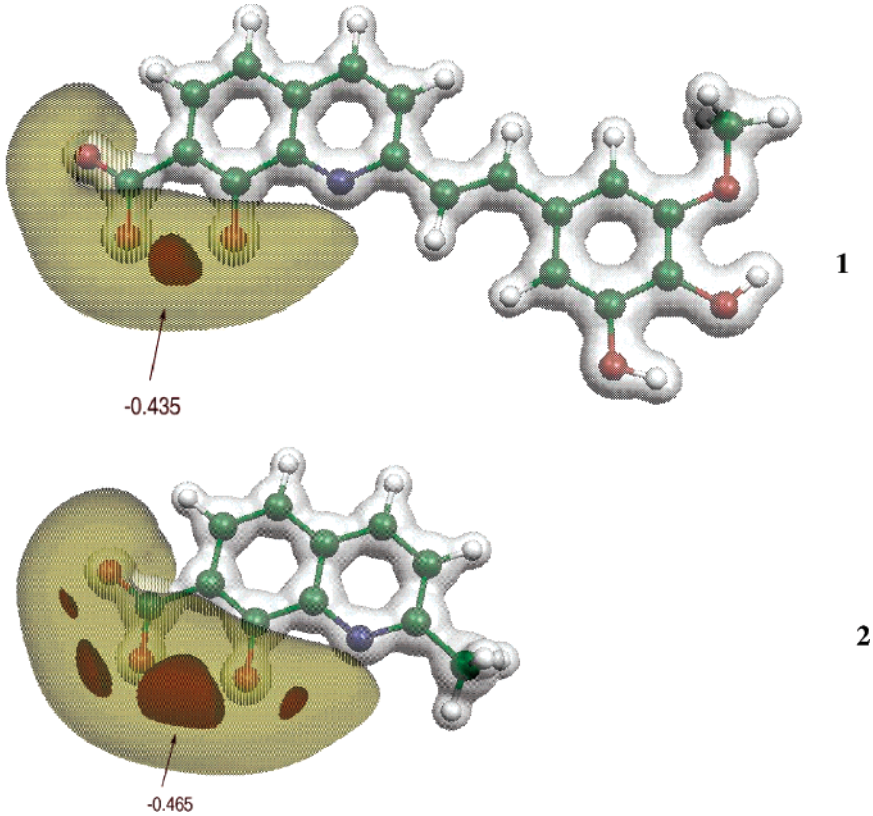

Figure 7. DFT electrostatic potentials of inhibitor **1** and its progenitor **2** in their dianionic state. Grey, yellow and red isosurfaces correspond to +0.20, −0.30, and −0.40 au, respectively. The arrows indicate the global minimum values of the electrostatic potential.

and three DMSO molecules per cluster were found in the crystal structure of **7**. Most of them (seven water molecules and two DMSO molecules) are located on disordered sites. In complex **7**, one DMSO molecule replaces one water molecule (Ow21 in Figure 3) connected to the corresponding Mg2 magnesium cation in complex **6**.

Structural comparison between the above complexes deserves the following comments. All Mg^{2+} cations are octahedrally coordinated whereas the Cu^{2+} ions have either a distorted tetrahedral (**6** and **7**) or pentahedral (for **5**) coordination. In the structures of **4** and **6**, the Mg−O distances are in the range of 1.958(2)−2.229(2) Å, the Mg−N bond lengths being significantly longer with an average value of 2.31 Å. In complex **6**, the Cu−O distances (1.968 Å in average) are systematically shorter than Cu−N (2.014 Å) ones. This trend, however, is not verified in the geometries of complex **5**, probably because of the coordination of a supplementary water molecule with a long Cu-Ow1 distance of 2.107(2) Å. In complex **4**, the Mg−Mg distance was found equal to 3.220(1) Å. As reported above, progenitor **2** acts as a tridentate chelator of two magnesium ions with a head-to-tail orientation of the ligands. In the mixed complex **6**, the copper cation imposes its preferential tetrahedral coordination. As can be seen in Figure 4, the sequestration of three Mg^{2+} ions is made possible by an original tridimensional arrangement of four chelators. The closest Mg−Mg distances remain, nevertheless, almost equal to that found in complex **4** [Mg1−Mg2 = 3.213(1) Å and Mg2−Mg3 = 3.184(1) Å]. Although structures of complexes **6** and **7** are very similar, their heterometallic cores slightly differ. In comparison to complex **6**, the Cu-O3 bond distance in **7** shortens (1.97 Å in **6** and 1.92 Å in **7**) whereas the Cu−N bond length increases from 2.02 Å (**6**) to 2.09 Å (**7**). The changes of the atomic bond distances and angles are displayed in Figure 5. Surprisingly, in complex **7**, the copper cation tends to adopt an octahedral coordination geometry characterized by an opening of the O3-Cu-O31 angle to 164.1° (142.01° in **6**) and a shortening of the Cu-O32/Cu-O33 distances (2.577/2.543 Å in **7** vs 3.135/3.051 Å in **6**). It is worthy to note that, in both complexes **6** and **7**, the N−Cu−N1 angle value does not change. The deformation of the oxometallic core of complex **7** implies that the Cu-Mg1/CuMg3 distances are shorter by about 0.2 Å in comparison to those found in complex **6**. However, the Mg−Mg distances are approximately the same in the two complexes.

The water molecules not involved in metal coordinations are regularly distributed in the empty space between the complex units for the three compounds. They stabilize the crystal lattices through multiple hydrogen bonds as shown in Figure 6. Given the relatively high number of extra water molecules per chemical formula in **4** (2 water molecules) and **6** (4 water molecules), these molecules are also interconnected and thus, form multiple bridges between the complex units. Complex **5** (1 extra water molecule), however, displays a much simple hydrogen bond network. In the three complexes, all cation-coordinated water molecules are involved in these hydrogen bonds. In **4** and **6**, the two carboxylato O1 and O2 atoms (Figure 3) are hydrogen-bonded to water molecules. In **5**, however, only O1 is involved in the intermolecular hydrogen-bonding system.

Theoretical Calculations. In order to quantify and further explore the metal-chelating property of progenitor **2**, theoretical calculations were performed in vacuo at the DFT level. The crystal atomic coordinates of the molecules were used in this case without any geometrical optimization. We first calculate the electronic properties of progenitor **2** in its dianionic state as it would interact with divalent cations during the crystallization process. Our previous studies of this molecule have revealed its zwitterionic character in the crystalline state.[34] In the present calculation, we removed the hydrogen atoms attached to the O3 center and to the quinoline N atom, respectively. For

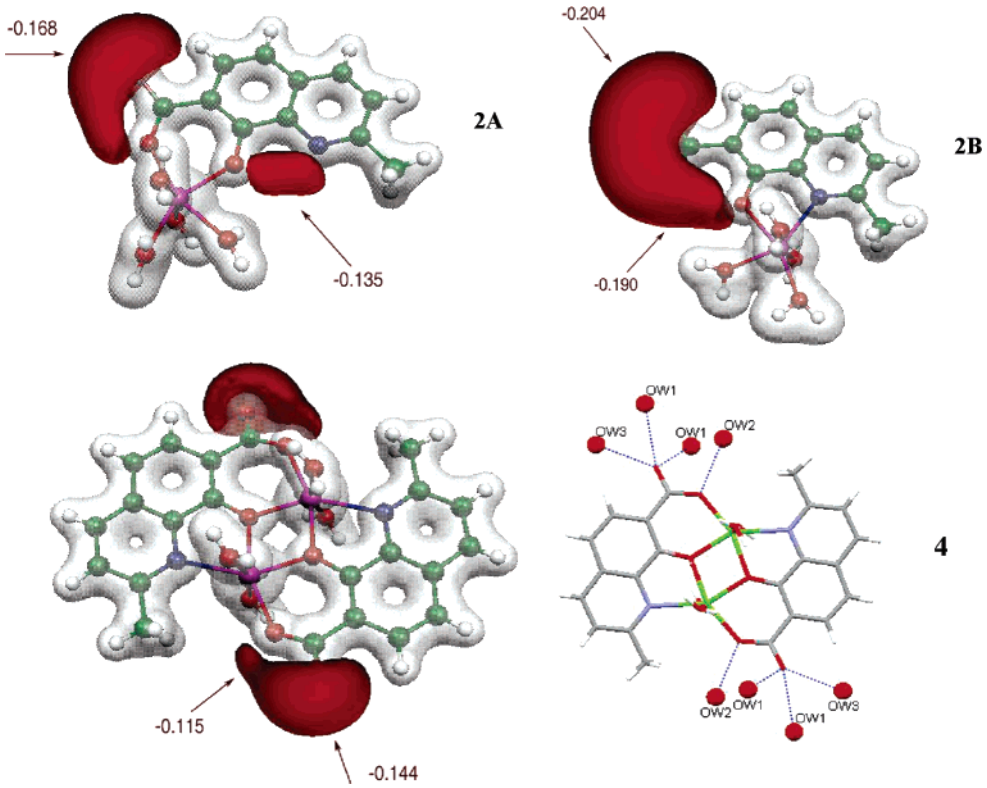

Figure 8. DFT electrostatic potential features of magnesium complexes **2A**, **2B**, and **4**. Grey and red isosurfaces correspond to +0.20 and −0.10 au, respectively. The arrows indicate the local minimum values of the electrostatic potential. The scheme at the right bottom shows the closest hydrogen bonds found in the crystal lattice of complex **4**.

the sake of comparison, we have also calculated the electrostatic potential of the inhibitor **1** also in the dianionic state. In Figure 7 are displayed the theoretical electrostatic potentials generated by the −2 charged molecules **1** and **2**. The high similarity of the electrostatic potentials generated by the whole inhibitor **1** and its quinoline half **2** is in excellent agreement with the outcomes of our previous atomic charges and NMR studies revealing the absence of any effect of electron delocalization through the ethylenic linker in **1**.[34] This also implicitly validates the choice of the quinoline half **2** for mimicking inhibitor **1** in the present metal complexation experiments. Taking a cutoff of −0.3 au, a large region of a negative electrostatic potential extends from the carboxyl group to the quinoline N atom. However, a negative hole of the electrostatic potential is found between O2 and O3 atoms with a global minimum reaching −0.435 in **1** and −0.465 au in **2** (see Figure 7). This shows that the most favorable site to sequester a cation lies between these two oxygen atoms. For both molecules, the second most probable chelating center is likely between O3 and quinoline N atoms because of the convenient cavity presented by this part of the ligand toward a metal cation. The local minimum values of the electrostatic potential found between O3 and N atoms are equal to −0.37 and −0.40 in **1** and **2**, respectively. All reported quinoline-based complex structures with different divalent metals (Co, Ni, Zn, Fe) support this prediction.[45,46,50,54]

Due to the physiological importance of Mg^{2+} cation and its well-known implication in the HIV-1 IN inhibition process, we focus on complex **4**. A DFT computation of the electronic structure of this complex was therefore performed. For the sake of comparison, we have also carried out separate calculations for hypothetical monomagnesium complexes of progenitor **2** in gas-phase. For this purpose, one magnesium cation was positioned between the carboxylato O2 and the phenoxo O3 atoms of the ligand **2** on one hand (hereafter complex **2A**), and between O3 and the quinoline N atom (complex **2B**) on the other hand. In each structure, two additional water molecules were artificially added to satisfy the sixfold coordination of Mg^{2+} cation. Only this part of the complex was geometrically optimized. Figure 8 depicts the theoretical electrostatic potentials generated around magnesium complexes **2A**, **2B**, and **4**, respectively. The red isopotential surface corresponds to the negative electrostatic potential (nucleophilic). By looking at the features of complexes **2A** and **2B**, it is worth noting that each time one chelating site [between O2 and O3 (site 1) or between O3 and N (site 2)] is fully occupied, the vacant site obviously displays a negative electrostatic potential minimum suitable for metal complexation.

TABLE 3: Total Electronic Energies (in au) and Mg-Binding Energies (BE = $E_c - E_s$ in kcal/mol) for the Three Magnesium Complexes 2A, 2B, and 4[a]

complex	E_c	E_s	BE	q_{Mg}
2A	−1209.5758	−1209.2330	−215.1	+1.534
2B	−1209.5444	−1209.2293	−197.7	+1.497
4	−2113.6972	−2113.3631	−209.7	+1.485

[a] The last column gives the Mg charges (in e unit) derived from the electrostatic potential.

As can be expected from atomic electronegativity considerations, the minimum at site 1 (−0.190 au in complex **2B**) is deeper than that found at site 2 (−0.135 au in complex **2A**). When the dimagnesium complex **4** is formed, a negative electrostatic potential region remains in the vicinity of O1 and O2 atoms. Accordingly, in the crystal lattice of complex **4**, these attractive centers give rise to multiple hydrogen bonds reported above and as also shown in the right-bottom of Figure 8. On the other hand, the electrostatic potential of **2A**, **2B** and **4** has been used to derive atomic charges based on the ChelpG method.[55] The magnesium charges are reported in Table 3. As can be expected, the highest magnesium charge is found for

complex **2A** where the cation resides in site 1. From the determinations of the total electronic energies of the complexes (E_c) and the sum (E_s) of the total energies of the isolated ligands and cations, it was possible to estimate the Mg-binding energies ($BE = E_c - E_s$) in each case. These values are reported in Table 3. The basis set superposition error (BSSE) was corrected using the Counterpoise method;[56] the values obtained for this BSSE correction are 0.0100, 0.0137, and 0.0209 au for complexes **2A**, **2B**, and **4**, respectively. The binding energies are around −200 kcal/mol, that is to say, approximately half of the experimental and theoretical hydration energies reported for Mg^{2+} cation.[57] The most stable configuration is found for monometallic complex **2A** where the magnesium cation is linked to both carboxyl and hydroxyl oxygen atoms (site 1). Comparatively, in complex **2B**, the site 2 involving chelation of O3 and N atoms exhibits the smallest binding energy of the Mg cation. These results are consistent with the marked preference of a carboxylate ligand to bind the "hard" Mg^{2+} cation.[52] However, only a weak difference in the complexation energy of 5.4 kcal/mol is found between complexes **2A** and **4**.

Conclusions

The present study sheds light on the HIV-1 IN inhibition process targeting divalent metal ion cofactor(s). Although the exact mechanism by which drug **1** and SQLs analogues exert their antiviral activity is still a matter of controversy,[29,30] several studies suggest that such compounds might inhibit IN at its interface with viral DNA and divalent metal(s), thereby preventing DNA-IN binding.[10,17,20] The ability for progenitor **2** to coordinate magnesium(II) and copper(II) ions is consistent with such a model. We have previously demonstrated through X-ray studies that drug **1** and its progenitor **2** crystallize both in the zwitterionic form.[34] This means that the carboxylate groups of these molecules are ionized, at least in the solid state. This phenomenon, highlighted by the large negative electrostatic potential isosurfaces surrounding the carboxylates,[34] clearly reinforces the chelating ability of these ligands toward metal cations. It is noteworthy that the original metallo-organic framework of the Mg(II) complex of **2** (**4**), consisting of a planar bis(μ-phenoxo)-bridged dimagnesium cluster in which the two metal centers are separated by ca. 3.2 Å, is reminiscent of the mechanism involving two metal ions (separated by ca. 3.9 Å) proposed by Beese and Steitz for the 3′-5′exonuclease reaction of *Escherichia coli* DNA polymerase I.[13] Note in this respect that a "two-metal" binding model was recently proposed as a potential mechanism of action of HIV-1 IN inhibitors.[58] On the other hand, the high chelating potency of progenitor **2** was also quantified through DFT-based ab initio calculations performed on the dimagnesium complex **4** and two hypothetical monomagnesium counterparts.

Understanding the mode of action of HIV-1 IN SQLs inhibitors may broaden considerably our current views on the design of more potent and more selective analogues. It also opens the possibility of tailoring new classes of HIV-1 IN inhibitors that could be exploited for the prophylaxis and treatment of AIDS.

Acknowledgment. The financial support of the CNRS, the European Synchrotron Radiation Facility (ESRF), Ecole Centrale Paris (ECP) and Université Paris XI is gratefully acknowledged.

Supporting Information Available: CIF files for the complexes reported in this paper. This material is available free of charge via the Internet at http://pubs.acs.org.

References and Notes

(1) De Clercq, E. *Med. Res. Rev.* **2002**, *22*, 531−565.
(2) De Clercq, E. *Nat. Rev. Drug Discovery* **2002**, *1*, 13−25.
(3) Turpin, J. A. *Expert Rev. Anti-Infect. Ther.* **2003**, *1*, 97−128.
(4) De Clercq, E. *J. Med. Chem.* **2005**, *48*, 1297−1313.
(5) Pommier, Y.; Neamati, N. *Adv. Virus Res.* **1999**, *52*, 427−458.
(6) Neamati, N.; Marchand, C.; Pommier, Y. *Adv. Pharmacol.* **2000**, *49*, 147−165.
(7) Neamati, N. *Expert Opin. Invest. Drugs* **2001**, *10*, 281−296.
(8) d'Angelo, J.; Mouscadet, J.-F.; Desmaële, D.; Zouhiri, F.; Leh, H. *Pathol. Biol.* **2001**, *49*, 237−246.
(9) Anthony, N. J. *Curr. Top. Med. Chem.* **2004**, *4*, 979−990.
(10) Pommier, Y.; Johnson, A. A.; Marchand, C. *Nat. Rev. Drug Discovery* **2005**, *4*, 236−248.
(11) Wolfenden, R.; Ridgway, C.; Young, G. *J. Am. Chem. Soc.* **1998**, *120*, 833−834.
(12) Williams, N. H.; Takasaki, B.; Wall, M.; Chin, J. *Acc. Chem. Res.* **1999**, *32*, 485−493.
(13) Beese, L. S.; Steitz, T. A. *EMBO J.* **1991**, *10*, 25−33.
(14) Blaskó, A.; Bruice, T. C. *Acc. Chem. Res.* **1999**, *32*, 475−484.
(15) Bujacz, G.; Alexandratos, J.; Wlodawer, A.; Merkel, G.; Andrake, M.; Katz, R. A.; Skalka, A. M. *J. Biol. Chem.* **1997**, *272*, 18161−18168.
(16) Pingoud, A.; Jeltsch, A. *Nucleic Acids Res.* **2001**, *29*, 3705−3727.
(17) Marchand, C.; Johnson, A. A.; Karki, R. G.; Pais, G. C. G.; Zhang, X.; Cowansage, K.; Patel, T. A.; Nicklaus, M. C.; Burke, T. R., Jr.; Pommier, Y. *Mol. Pharmacol.* **2003**, *64*, 600−609.
(18) Sechi, M.; Bacchi, A.; Carcelli, M.; Compari, C.; Duce, E.; Fisicaro, E.; Rogolino, D.; Gates, P.; Derudas, M.; Al-Mawsawi, L. Q.; Neamati, N. *J. Med. Chem.* **2006**, *49*, 4248−4260.
(19) Goldgur, Y.; Dyda, F.; Hickman, A. B.; Jenkins, T. M.; Craigie, R.; Davies, D. R. *Proc. Natl. Acad. Sci. U.S.A.* **1998**, *95*, 9150−9154.
(20) Lins, R. D.; Straatsma, T. P.; Briggs, J. M. *Biopolymers* **2000**, *53*, 308−315.
(21) Mekouar, K.; Mouscadet, J.-F.; Desmaële, D.; Subra, F.; Leh, H.; Savouré, D.; Auclair, C.; d'Angelo, J. *J. Med. Chem.* **1998**, *41*, 2846−2857.
(22) Zouhiri, F.; Mouscadet, J.-F.; Mekouar, K.; Desmaële, D.; Savouré, D.; Leh, H.; Subra, F.; Le Bret, M.; Auclair, C.; d'Angelo, J. *J. Med. Chem.* **2000**, *43*, 1533−1540.
(23) Ouali, M.; Laboulais, C.; Leh, H.; Gill, D.; Desmaële, D.; Mekouar, K.; Zouhiri, F.; d'Angelo, J.; Auclair, C.; Mouscadet, J.-F.; Le Bret, M. *J. Med. Chem.* **2000**, *43*, 1949−1957.
(24) Ouali, M.; Laboulais, C.; Leh, H.; Gill, D.; Xhuvani, E.; Zouhiri, F.; Desmaële, D.; d'Angelo, J.; Auclair, C.; Mouscadet, J.-F.; Le Bret, M. *Acta Biochim. Pol.* **2000**, *47*, 11−22.
(25) Burdujan, R.; d'Angelo, J.; Desmaële, D.; Zouhiri, F.; Tauc, P.; Brochon, J.-C.; Auclair, C.; Mouscadet, J.-F.; Pernot, P.; Tfibel, F.; Enescu, M.; Fontaine-Aupart, M.-P. *Phys. Chem. Chem. Phys.* **2001**, *3*, 3797−3804.
(26) Zouhiri, F.; Desmaële, D.; d'Angelo, J.; Ourevitch, M.; Mouscadet, J.-F.; Leh, H.; Le Bret, M. *Tetrahedron Lett.* **2001**, *42*, 8189−8192.
(27) Polanski, J.; Zouhiri, F.; Jeanson, L.; Desmaële, D.; d'Angelo, J.; Mouscadet, J.-F.; Gieleciak, R.; Gasteiger, J.; Le Bret, M. *J. Med. Chem.* **2002**, *45*, 4647−4654.
(28) Bénard, C.; Zouhiri, F.; Normand-Bayle, M.; Danet, M.; Desmaële, D.; Leh, H.; Mouscadet, J.-F.; Mbemba, G.; Thomas, C.-M.; Bonnenfant, S.; Le Bret, M.; d'Angelo, J. *Bioorg. Med. Chem. Lett.* **2004**, *14*, 2473−2476.
(29) Bonnenfant, S.; Thomas, C.-M.; Vita, C.; Subra, F.; Deprez, E.; Zouhiri, F.; Desmaële, D.; d'Angelo, J.; Mouscadet, J.-F.; Leh, H. *J. Virol.* **2004**, *78*, 5728−5736.
(30) Deprez, E.; Barbe, S.; Kolaski, M.; Leh, H.; Zouhiri, F.; Auclair, C.; Brochon, J.-C.; Le Bret, M.; Mouscadet, J.-F. *Mol. Pharmacol.* **2004**, *65*, 85−98.
(31) Ma, X. H.; Zhang, X. Y.; Tan, J. J.; Chen, W. Z.; Wang, C. X. *Acta Pharm. Sin.* **2004**, *25*, 950−958.
(32) Zouhiri, F.; Danet, M.; Bénard, C.; Normand-Bayle, M.; Mouscadet, J.-F.; Leh, H.; Thomas, C.-M.; Mbemba, G.; d'Angelo, J.; Desmaële, D. *Tetrahedron Lett.* **2005**, *46*, 2201−2205.
(33) Normand-Bayle, M.; Bénard, C.; Zouhiri, F.; Mouscadet, J.-F.; Leh, H.; Thomas, C.-M.; Mbemba, G.; Desmaële, D.; d'Angelo, J. *Bioorg. Med. Chem. Lett.* **2005**, *15*, 4019−4022.
(34) Firley, D.; Courcot, B.; Gillet, J.-M.; Fraisse, B.; Zouhiri, F.; Desmaële, D.; d'Angelo, J.; Ghermani, N. E. *J. Phys. Chem. B* **2006**, *110*, 537−547.
(35) Altomare, A.; Burla, M. C.; Camalli, M.; Cascarano, G. L.; Giacovazzo, C.; Guagliardi, A.; Moliterni, A. G. G.; Polidori, G.; Spagna, R. *J. Appl. Cryst.* **1999**, *32*, 115−119.
(36) Sheldrick, G. M. *SHELX97*, Programs for Crystal Structure Analysis (Release 97−2), University of Göttingen, Göttingen, Germany, 1998.
(37) Farrugia, L. J. *J. Appl. Crystallogr.* **1999**, *32*, 837−838.

(38) a) Spek, A. L. *Acta Crystallogr.* **1990**, *A46*, C34. b) Spek, A. L. *PLATON, A Multipurpose Crystallographic Tool*; Utrecht University: Utrecht, The Netherlands, 1998.

(39) Cooper, R. I.; Gould, R. O.; Parsons, S.; Watkin, D. J. *J. Appl. Crystallogr.* **2002**, *35*, 168−174.

(40) Frisch, M. J.; Trucks, G. W.; Schlegel, H. B.; Scuseria, G. E.; Robb, M. A.; Cheeseman, J. R.; Montgomery, J. A., Jr.; Vreven, T.; Kudin, K. N.; Burant, J. C.; Millam, J. M.; Iyengar, S. S.; Tomasi, J.; Barone, V.; Mennucci, B.; Cossi, M.; Scalmani, G.; Rega, N.; Petersson, G. A.; Nakatsuji, H.; Hada, M.; Ehara, M.; Toyota, K.; Fukuda, R.; Hasegawa, J.; Ishida, M.; Nakajima, T.; Honda, Y.; Kitao, O.; Nakai, H.; Klene, M.; Li, X.; Knox, J. E.; Hratchian, H. P.; Cross, J. B.; Bakken, V.; Adamo, C.; Jaramillo, J.; Gomperts, R.; Stratmann, R. E.; Yazyev, O.; Austin, A. J.; Cammi, R.; Pomelli, C.; Ochterski, J. W.; Ayala, P. Y.; Morokuma, K.; Voth, G. A.; Salvador, P.; Dannenberg, J. J.; Zakrzewski, V. G.; Dapprich, S.; Daniels, A. D.; Strain, M. C.; Farkas, O.; Malick, D. K.; Rabuck, A. D.; Raghavachari, K.; Foresman, J. B.; Ortiz, J. V.; Cui, Q.; Baboul, A. G.; Clifford, S.; Cioslowski, J.; Stefanov, B. B.; Liu, G.; Liashenko, A.; Piskorz, P.; Komaromi, I.; Martin, R. L.; Fox, D. J.; Keith, T.; Al-Laham, M. A.; Peng, C. Y.; Nanayakkara, A.; Challacombe, M.; Gill, P. M. W.; Johnson, B.; Chen, W.; Wong, M. W.; Gonzalez, C.; Pople, J. A. *Gaussian 03*, revision B.04; Gaussian, Inc: Wallingford, CT, 2004.

(41) Hohenberg, P.; Kohn, W. *Phys. Rev.* **1964**, *136*, B864−B871.

(42) Kohn, W.; Sham, L. *Phys. Rev.* **1965**, *140*, A1133−A1138.

(43) Lee, C.; Yang, W.; Parr, R. G. *Phys. Rev. B* **1988**, *37*, 785−789.

(44) Becke, A. D. *J. Chem. Phys.* **1993**, *98*, 5648−5652.

(45) Okabe, N.; Muranishi, Y. *Acta Crystallogr.* **2002**, *C58*, m475−m477.

(46) Okabe, N.; Muranishi, Y. *Acta Crystallogr.* **2002**, *E58*, m352−m353.

(47) Francis, S.; Muthiah, P. T.; Rychlewska, U.; Warźajtis, B. *Acta Crystallogr.* **2004**, *E60*, m137−m139.

(48) Vincent, J. B.; Folting, K.; Huffman, J. C.; Christou, G. *Inorg. Chem.* **1986**, *25*, 996−999.

(49) Ovcharenko, V. I.; Vostrikova, K. E.; Podoplelov, A. V.; Romanenko, G. V.; Ikorskii, V. N.; Reznikov, V. A. *Polyhedron* **1997**, *16*, 1279−1289.

(50) Burnett, M. N.; Johnson, C. K. *ORTEPIII, Oak Ridge Thermal Ellipsoid Plot Program for Crystal Structure Illustrations*; Report ORNL-6895; Oak Ridge National Laboratory: Oak Ridge, TN, 1996.

(51) Okabe, N.; Muranishi, Y. *Acta Crystallogr.* **2003**, *E59*, m244−m246.

(52) In *The Biological Chemistry of the Elements*; Fraústo da Silva, J. J. R.; Williams, R. J. P.; Eds.; Clarendon Press: Oxford, 1994; pp 31−36.

(53) Edwards, C. F.; Griffith, W. P.; White, A. J. P.; Williams, D. J. *Polyhedron* **1992**, *11*, 2711−2712.

(54) Okabe, N.; Muranishi, Y. *Acta Crystallogr.* **2003**, *E59*, m220−m222.

(55) Breneman, C. M.; Wiberg, K. B. *J. Comput. Chem.* **1990**, *11*, 361−373.

(56) Boys, S. F.; Bernardi, F. *Mol. Phys.* **1970**, *19*, 553−566.

(57) Reynisson, J.; Steenken, S. *J. Mol. Struct. (THEOCHEM)* **2003**, *635*, 133−139.

(58) Kawasuji, T.; Fuji, M.; Yoshinaga, T.; Sato, A.; Fujiwara, T.; Kiyama, R. *Bioorg. Med. Chem.* **2006**, *14*, 8420−8429.